

Simple model for heterogeneous flows of yield stress fluids

Guillemette Picard* and Armand Ajdari

Laboratoire de Physico-Chimie Théorique, UMR CNRS 7083, ESPCI, 10 Rue Vauquelin, F-75231 Paris Cedex 05, France

Lydéric Bocquet

Laboratoire de Physique de l'ENS de Lyon, UMR CNRS 5672, 46 Allée d'Italie, 69364 Lyon Cedex, France

François Lequeux

Laboratoire de Physico-Chimie Macromoléculaire, UMR CNRS 7615, ESPCI, 10 Rue Vauquelin, F-75231 Paris Cedex 05, France

(Received 7 June 2002; published 5 November 2002)

Various experiments evidence spatial heterogeneities in sheared yield stress fluids. To account for heterogeneities in the velocity gradient direction, we use a simple model corresponding to a nonmonotonic local flow curve and study a simple shear geometry. Different types of boundary conditions are considered. Under controlled macroscopic shear stress Σ , we find homogeneous flow in the bulk and a hysteretic macroscopic stress–shear-rate curve. Under controlled macroscopic shear rate $\dot{\Gamma}$, shear banding is predicted within a range of values of $\dot{\Gamma}$. For small shear rates, stick-slip can also be observed. These qualitative behaviors are robust to changes in the boundary conditions.

DOI: 10.1103/PhysRevE.66.051501

PACS number(s): 83.10.Tv, 83.60.La, 83.60.Rs, 83.10.Gr

I. INTRODUCTION

Complex materials, such as concentrated colloidal suspensions, gels, or foams, often exhibit exotic rheological behavior at low shear [1–11], very different from the Newtonian linear response characterized by a stress Σ linearly proportional to the shear rate $\dot{\Gamma}$ (in scalar language). A term often coined for some of these behaviors is that of “yield stress fluids.” Although often loosely used, it most of the time describes fluids that have one or both of the following properties: when one looks at the steady state flow curve $\Sigma(\dot{\Gamma})$ at low shear, (i) the stress Σ tends to a finite value Σ_Y when the shear rate goes to zero; (ii) no flowing steady state solution exists for stresses smaller than a value Σ_0 . Consequently, at low stresses, the system does not really flow, and these “pastes” often display physical aging in a way rather similar to structural glasses.

A traditional way to apprehend this *macroscopic* rheological nonlinear behavior is to suppose the existence of a *local* relation between the *local* stress σ and the *local* shear rate $\dot{\gamma}$ of one of the forms I to IV in Fig. 1. Classically again, I to III being monotonic can lead to a homogeneous flow so that the macroscopic response is identical to the local flow curve: while II and III correspond to genuine yield stress fluids satisfying both (i) and (ii) above [with $\Sigma_0 = \Sigma_Y = \sigma(\dot{\gamma}=0)$], I yields a power law fluid behavior $\Sigma = A\dot{\Gamma}^\alpha$ which can be experimentally very difficult to tell apart from the yield stress behaviors II and III if α is small. It is classically argued, on the other hand, that the decreasing branch of IV ($d\Sigma/d\dot{\Gamma} < 0$) cannot lead to the corresponding homogeneous situation, as such a flow is unstable with respect to the formation of “shear bands” or domains flowing at different lo-

cal shear rates. This statement is usually substantiated by a simple argument invoking inertial terms (see, for instance, [12]). This type of banding is referred to as “gradient banding” as opposed to “vorticity banding” (coexistence of domains flowing at different local shear stress and common shear rate).

The question then arises of the structure of the heterogeneous flow pattern observed in these conditions (curve IV, gradient banding), of its stability (i.e., are there always steady-state solutions?), and of the resulting macroscopic flow curve $\Sigma(\dot{\Gamma})$ for the steady-state solutions. Investigating this problem in generic terms is very difficult as many underlying dynamical laws involving an unlimited number of “hidden” variables can generate local equations such as IV. In this paper, to make progress, we consequently make a specific choice for this underlying dynamics, which we justify now.

Formally, taking the vertical $\dot{\gamma}=0$ axis as part of the local flow curve, the problem is very similar to the analysis of flow-induced or flow-assisted “phase” transitions for sys-

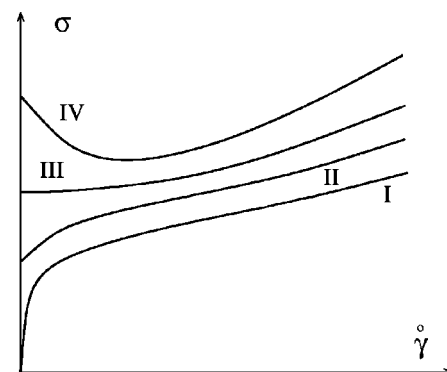


FIG. 1. Schematic representation of possible local steady-state curve $\sigma(\dot{\gamma})$ generating a macroscopic yield stress fluid behavior.

*Electronic address: guillemette@turner.pct.espci.fr

tems with a local nonmonotonic relationship $\sigma(\dot{\gamma})$. For some systems, the change in rheological properties can be ascribed to a structural phase transition occurring under flow: Ramos *et al.* with lyotropic hexagonal phases [2], Diat *et al.* with onions [4], and Britton and Callaghan [1] and Berret *et al.* with wormlike micelles [3] observe a phase transition, and the coexistence of two well defined phases. Such behaviors are quite reminiscent of equilibrium phase transitions, although no general principle applies *a priori* in such out of equilibrium situations [13]. The identification of structural differences between the flowing phases then provides a guide as to what are the most likely relevant local variables beyond the rheological ones: a (nonconserved) nematic order parameter, the (conserved) concentration of a constituent, etc. Related theoretical descriptions have thus tried to describe the coupling between this order parameter and flow in order to obtain a selection criterion for the flow pattern and the resulting macroscopic rheological behavior [13–19].

However, for many yield stress fluids there is no obvious structural difference between the coexisting flowing phases: experimental reports often describe “shear bands” of a flowing “phase” in a stationary “phase” with no clear structural or textural difference between the two parts of the system. Such “soft glassy materials” [8] include gels, pasty systems, concentrated glassy suspensions, and so on. One may cite the work by Raynaud *et al.* [7], where banding is observed in a suspension of bentonite and the interface between the bands is in the velocity-vorticity plane (gradient banding): the system is sheared within a band at the inner moving cylinder, while the rest of the sample remains unsheared. Laponite suspensions also undergo banding for a certain range of imposed shear rates, a range for which the shear stress is almost constant [10]. Noticeably, for a range of lower shear rates stick-slip is observed in this system: a layer reversibly fractures and reheals, showing stationary oscillations in the measured stress. Eventually, one may note that inhomogeneous velocity profiles are also observed in sheared foams [5] and granular pastes [11].

For these systems with no clearly identified structural variable that would distinguish coexisting phases, there is much less guidance for building models. Still, banding is likely to originate from the same basic physical mechanism as for phase separating fluids [20]. Models have therefore been derived along similar lines, which differ by the choice of the hidden variable (equivalent to the order parameter) and of its dynamics [20,22]. In addition, or alternatively, gradient terms were included in the nonmonotonic intrinsic law $\sigma(\dot{\gamma})$ [12,21].

In the present paper we follow the route initiated by Derec *et al.* [23], which has been shown to be a simple though useful guide to understand the interplay between nonlinear rheology and aging properties for yield stress fluids characterized by local flow curves of types I to III [23,24]. In the present work we adapt it to describe local flow curves of type IV, and to take into account spatial heterogeneities.

The essence of the model of [23] is to describe the local state of the system by a single scalar variable that is for convenience taken to be the local relaxation frequency of the

stress (called the “fluidity”), as expressed by a Maxwell equation $\partial_t \sigma = -a(t)\sigma + \dot{\gamma}$ (stress has been rescaled so that the elastic modulus is 1). Then the evolution of the fluidity $a(t)$ results from the competition between (i) *aging*—relaxation rates in the system decrease during the spontaneous evolution of the pasty system, this evolution being itself slower and slower as time passes; and (ii) *flow-induced rejuvenation*—flow induces rearrangements in the system, which in turn increase the fluidity of the system as a feedback mechanism [9,24–26]. This competition results in an equation for a that supplements the Maxwell one: $\partial_t a = -f(a) + g(a, \sigma, \dot{\gamma})$, with f and g positive functions.

Here, to address the question at hand, we focus on choices for f and g leading to local flow curves (local steady states) with a decreasing branch at low values of $\dot{\gamma}$, and we attempt to describe spatial heterogeneities, through a simple diffusion term $D\Delta a$ in the equation describing the evolution of a .

We then study the flow patterns in a simple shear geometry for such a system, when it is driven at either imposed macroscopic shear stress Σ or imposed macroscopic shear rate $\dot{\Gamma}$, and deduce the resulting macroscopic rheological behavior. We will on the way provide analytical and numerical arguments, using when necessary explicit choices for f and g , and pinpoint the role of the boundary conditions. In particular we will show that the model accounts for the following features.

(1) When Σ is imposed, the flow curve jumps in a hysteretic fashion between two branches: one corresponds to no flow but for a wall layer in the vicinity of the walls; the other corresponds to a fully fluidized situation.

(2) When the global shear rate $\dot{\Gamma}$ is imposed, shear banding can occur, as well as sometimes a stick-sliplike oscillating behavior at small shear rate that corresponds to a localized oscillation of the fluidity.

These features will be analyzed in the context of experimental results.

The paper is organized as follows. We recall in Sec. II the basic ingredients of the model in Ref. [23] and propose a generalization to account for inhomogeneities in the system. The homogeneous case is detailed in Sec. III and the stability of the homogeneous solutions is discussed. Heterogeneous solutions are considered in Secs. IV and V. In Sec. IV the controlled stress situation is considered, while in Sec. V the global shear rate is imposed. In Sec. VI, choices made in building the model and the influence of the boundary conditions are discussed.

II. MODEL AND GEOMETRY

In this section we define more clearly the model and the geometry we are going to study, following the physical arguments given in the Introduction. In Sec. II A, we specify further the functions f and g , in Sec. II B we describe the geometry considered and the corresponding description of heterogeneities in the equations, in Sec. II C we define the boundary conditions for both velocity and fluidity, and we summarize in Sec. II D by recalling the resulting set of equations.

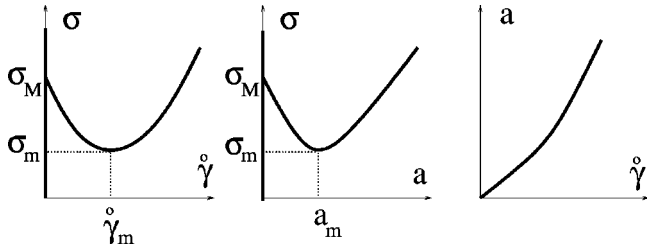


FIG. 2. Schematic drawing of the local steady-state flow curve $\sigma(\dot{\gamma}), \sigma(a), \dot{\gamma}(a)$.

A. Accounting for a nonmonotonic local flow curve

From the Introduction, we start with the model of [23], devised for homogeneous situations:

$$\partial_t \sigma = -a\sigma + \dot{\gamma},$$

$$\partial_t a = -f(a) + g(a, \sigma, \dot{\gamma}). \quad (1)$$

For the sake of explicitness, and with loss of generality, it will often be useful to restrict the choices for the functions f and g appearing in Eq. (1). This is particularly true for the flow-induced rejuvenation term $g(a, \sigma, \dot{\gamma})$ which can take many forms.

Following again Derec *et al.* [23], we take forms corresponding to low values of the stress, shear rate, and fluidity, so that power laws may express a kind of expansion of more general functions. Also, a being a positive scalar, the direction of shear is of no influence so one expects $g(a, \sigma, \dot{\gamma}) = g(a, -\sigma, -\dot{\gamma})$. A simple solution is then $g(a, \sigma, \dot{\gamma}) = h(a)\sigma\dot{\gamma}$.

Then, following the Introduction, we want the steady-state flow curve $\sigma(\dot{\gamma})$ to have a decreasing branch for small but nonzero values of $\dot{\gamma}$ (as sketched in Fig. 2). In that case, the steady-state solutions of the system (1) consist of the vertical axis ($a=0, \dot{\gamma}=0, \sigma$ arbitrary), and solutions given by $\sigma(a) = [f(a)/ah(a)]^{1/2}$ when expressed in the plane s, a . The function $a(\dot{\gamma})$ is a monovalued increasing function, whereas $\sigma(a)$ is multivalued, decreasing for small values of a and then increasing for larger values. The requirements are thus that $f(a)/ah(a)$ has a negative derivative for $0 < a < a_m$ and a positive one for $a_m < a$. The minimum thus reached for a_m corresponds to the minimal value of the stress $\sigma_m = [f(a_m)/a_m h(a_m)]^{1/2}$. Eventually, as for curve IV in Fig. 1, σ tends toward a finite value when $\dot{\gamma}$ goes to zero, which we call σ_M .

When numerical calculation proves necessary to analyze the evolution of the system, we make even more explicit choices regarding f and h , which must of course satisfy the above requirements. We use the simple choice $f(a) = ra^2 + a^4$, $h(a) = r'a + a^2$ with r and r' arbitrary numbers that we vary to check the robustness of our conclusions. That $f(a)$ scales as a^2 for small values of a gives a spontaneous relaxation of a as the inverse of the elapsed time, a situation often referred to as “full aging” (see [23]).

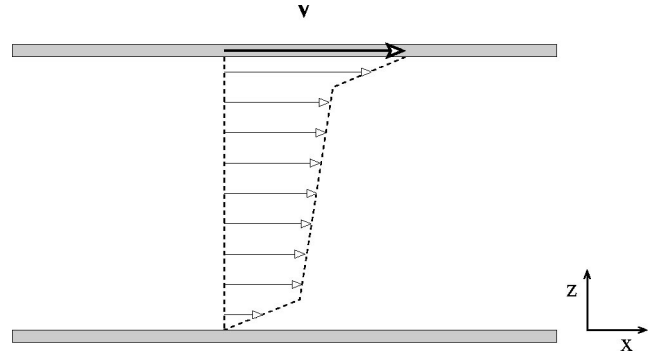


FIG. 3. Geometry: simple shear along x , variations along z only. The flow can be heterogeneous; the example depicted here corresponds to a low fluidity in the bulk and wall layers of higher fluidity close to the wall.

B. Incorporating heterogeneities: Geometry and model

In principle, a general description of heterogeneous flows implies complex algebra describing the evolution of scalar and tensorial quantities through convected derivatives, and writing various conservation equations (for mass, momentum, etc.). We focus here on the simplest flow geometry (simple shear), allowing only variations along one direction, perpendicular to flow and vorticity.

More precisely, we consider our complex fluid to be bounded by two parallel plates located at $z=0$ and $z=H$ (see, e.g., Fig. 3). The top plate moves along x at a velocity V , while the bottom one is immobile, so that the macroscopic shear rate is $\dot{\Gamma} = V/H$. In this situation we consider laminar flows along x , where the local variables $\sigma = \sigma_{xz}$, $\dot{\gamma}$, and a depend only on z (i.e., not on x and y).

Neglecting acceleration (inertial) terms is a common assumption for such (highly viscous) fluids on the ground of a low Reynolds number. This in general makes the stress divergence free, but in the present geometry it results in the stress being spatially constant so that it is no longer a local variable. We will in this paper make this assumption of fast momentum diffusion, while keeping in mind that by doing so we formally suppress a “mechanical instability” that destabilizes into bands any homogeneous flow solution corresponding to a decreasing part of the local flow curve $d\sigma/d\dot{\gamma} < 0$ (see, e.g., [12,20,27]). In this framework, the local stress depends solely on time, and is identical to the macroscopic stress $\sigma(z, t) = \sigma(t) = \Sigma(t)$.

Now in order to discuss spatial heterogeneities we need to account for the effect on the dynamics of a heterogeneous value of the fluidity. Again, for the sake of simplicity, we model this as a diffusion process in the evolution of the fluidity and correspondingly add a $D\nabla^2 a$ diffusion term to the second equation of (1). This choice corresponds to a picture in which the system is fluidized in a localized region; this triggers spontaneous local relaxations which themselves tend to fluidize the neighborhood of the initial region. Accordingly, we take the “diffusive coefficient” to be a positive constant. A negative value would generate local, small wavelength instabilities that destabilize homogeneous flow even at high shear rates. As we focus here on the instability gener-

ated by the nonmonotonic branch of the local flow curve, and in line with experimental observations [7,9] of homogeneous flow at high shear, we discard this possibility here. In addition, we do not consider other terms formally allowed by symmetry such as $(\nabla a)^2$.

The system is therefore described by the coupled equations

$$\partial_t \sigma(t) = -a(z,t)\sigma(t) + \dot{\gamma}(z,t),$$

$$\partial_t a(z,t) = -f(a(z,t)) + h(a(z,t))\sigma(t)\dot{\gamma}(z,t) + D\partial_{zz}^2 a(z,t). \quad (2)$$

One may note that in its present form the equation for the fluidity is close to the equation for the granular temperature obtained within the granular hydrodynamics of inelastic beads [28]: the spatial diffusion term accounts in the latter case for “heat” diffusion (according to Fourier law) and the “aging” term corresponds to the energy dissipation term (due to the inelasticity of collisions), which drives the granular material toward a state of zero temperature. Eventually, the granular temperature is indeed a measure of the local fluidity of the granular material.

An important comment is also that the diffusion coefficient D that we took constant here could in principle be a function of a . This would affect the length scale appearing from the competition of $f(a)$ and $D\partial_{zz}^2 a$. If, as in the example at the end of the previous subsection, $f(a) \sim a^2$ for small a , then this length scale depends on the actual value of a : $(D/a)^{1/2}$, indicating algebraic tails for spatial structures of low fluidity.

C. Boundary conditions

The equation for the fluidity and velocity have to be supplemented by boundary conditions at the confining walls at $z=0$ and $z=H$.

We here exclude any direct wall slippage and assume the plates to be sufficiently rough for the plate velocity to be equal to the limit velocity in the fluid approaching the plate (no slip velocity). This is equivalent to

$$\int_0^H dz \dot{\gamma}(z,t) = V(t) = \dot{\Gamma}(t)H. \quad (3)$$

It is important to point out that this hydrodynamic condition is not sufficient: a boundary condition for the fluidity equation is also required. How the walls affect the density, order, and relaxation processes of the fluid in their vicinity is obviously a complex problem with many aspects to it, even for simple liquids [29]. A smooth flat wall can enhance ordering; a rough or chemically disordered one can on the contrary locally disorganize the fluid (relative to what happens in the bulk). The consequences of these on the local relaxation rates being far from trivial [30], we choose here to investigate two limiting simple cases that hopefully bracket the true behavior: (i) a fixed fluidity at the wall

$$a(z=0) = a(z=H) = a_w, \quad (4)$$

and (ii) a zero gradient condition

$$\partial_z a|_{z=0,H} = 0. \quad (5)$$

D. Summary

We summarize here the equations that we will use in the remainder of the paper:

$$\partial_t \Sigma = -a\Sigma + \dot{\gamma},$$

$$\partial_t a = -f(a) + h(a)\Sigma\dot{\gamma} + D\partial_{zz}^2 a,$$

$$\int_0^H dz \dot{\gamma}(z,t) = V = \dot{\Gamma}H,$$

$$a|_{z=0,H} = a_w \quad \text{or} \quad \partial_z a|_{z=0,H} = 0, \quad (6)$$

where $\Sigma(t), \dot{\Gamma}(t)$ are global variables whereas $a(z,t)$ and $\dot{\gamma}(z,t)$ are local ones. When explicit choices are necessary to study the corresponding dynamics, we will use $f(a) = ra^2 + a^4$ and $h(a) = r'a + a^2$.

Let us recall that by neglecting the inertial terms we formally suppress the “mechanical instability” that destabilizes the decreasing branch $d\sigma/d\gamma < 0$.

Numerical method. For various cases, it is difficult or impossible to get analytical results and numerical calculation becomes necessary. The evolution equations for the stress and the fluidity, Eq. (6), have been solved numerically using a pseudospectral method, together with a Runge-Kutta integrator [31]. This technique integrates the diffusion part of the time equation for the fluidity in Fourier space, while the nonlinear part is solved in real space. Special care has been taken to avoid aliasing of the solutions. A standard fast Fourier transform algorithm is used for the forward and backward transformations between real and Fourier space.

We wish to use Eqs. (6) to deduce the macroscopic behavior of the system, to analyze the conditions for the existence of a steady state, and to describe the features of the flow. Note that the boundaries appear explicitly, as potential heterogeneities, so that most of the time the structure close to the boundaries will be different from the one in the bulk, allowing the walls to nucleate new “phases” before the bulk. Actually, the absence of noise terms in these equations suppresses the equivalent of homogeneous nucleation in thermodynamics problems. We briefly comment upon the addition of noise when it plays a significant role. In the following three sections, we first consider briefly the formal case of a homogeneous behavior (Sec. III); we then analyze the simpler case of the response to a fixed stress Σ (Sec. IV), before turning to the more complex case of a fixed global shear rate $\dot{\Gamma}$ (Sec. V).

III. HOMOGENEOUS BEHAVIOR

We first analyze briefly the homogeneous case, where we impose the requirement that the fluidity $a(t)$ is independent of z , so that Σ and $\dot{\Gamma}$ are similar to σ and $\dot{\gamma}$. Although slightly redundant with previous discussions of the flow

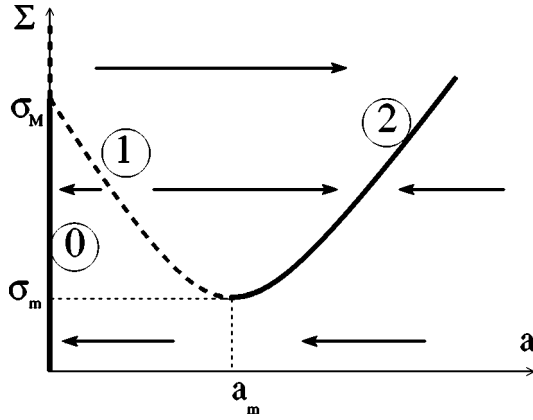


FIG. 4. Schematic description of the evolution of a at fixed stress (horizontal arrows). Stable steady-state branches are in bold; unstable ones in dashed lines.

curve, this analysis will highlight the potential differences between the stability analyses at fixed stress and fixed shear rate. These differences naturally result from the fact that Σ and $\dot{\Gamma}$ are treated on a different footing in Eq. (1).

As previously stated, steady-state solutions consist of three branches.

Branch 0: $\dot{\Gamma} = 0$, $a = 0$, Σ arbitrary. This corresponds to a frozen, nonflowing system.

Branch 1: $a < a_m$, $\dot{\Gamma} < \dot{\gamma}_m = a_m \sigma_m$, and Σ is a decreasing function of both a and $\dot{\Gamma}$.

Branch 2: $a > a_m$, $\dot{\Gamma} > \dot{\gamma}_m$, and Σ is an increasing function of both a and $\dot{\Gamma}$, from σ_m up to ∞ .

The three solutions (or branches) of fluidity are schematically plotted in the (Σ, a) plane in Fig. 4 [the $\Sigma(\dot{\Gamma})$ plot has a similar aspect and is identical to the left curve in Fig. 2]. We will use the notation $a_1(\Sigma)$ and $a_2(\Sigma)$ to designate branches 1 and 2 [the two roots of $\Sigma^2 = f(a)/ah(a)$].

A. Imposed stress Σ

The evolution of a homogeneous system at fixed $\Sigma = \sigma$ is truly simple as the Maxwell model yields $\dot{\Gamma} = a\Sigma$ which can be injected in the equation describing the fluidity, so that the evolution of the system is completely described by the sole differential equation

$$\frac{da}{dt} = -\frac{dV_\Sigma}{da}(a), \quad (7)$$

where the “effective potential” V_Σ is

$$V_\Sigma(a) = \int_0^a da' [f(a') - a'h(a')\Sigma^2]. \quad (8)$$

The above equation describes the relaxation of a in the potential V_Σ . Depending on the value of the imposed Σ , this potential has either one or three extrema: for $\Sigma < \sigma_m$, $a = 0$ is the only minimum; for $\sigma_M > \Sigma > \sigma_m$, V_Σ has two minima, $a = 0$ and $a = a_2(\Sigma)$ and a single maximum $a = a_1(\Sigma)$; and for $\Sigma > \sigma_M$, $a = a_2(\Sigma)$ is the only minimum.

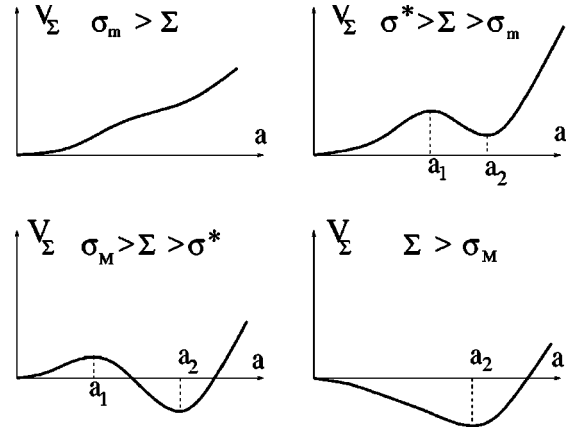


FIG. 5. Effective potential $V_\Sigma(a)$ for the evolution of $a(t)$ in the homogeneous case. Depending on the actual value of Σ , V_Σ has one or two minima.

Linear stability immediately results (see Fig. 4), as the system falls in the potential $V_\Sigma(a)$ along the instantaneous slope at point $a(t)$ (see Fig. 5).

Branch 0 is stable for $\Sigma < \sigma_M$ so that the system evolves to this frozen situation whenever the stress is too weak, $\Sigma < \sigma_m$. At long times the system typically creeps but does not flow, $\dot{\Gamma}(t) = a(t)\Sigma$ with $a(t)$ decreasing (typically algebraically in time) to 0. For example, with the explicit values of f and h proposed above, one has $a(t) \sim 1/t$ so that $\Gamma(t) \sim \Sigma \ln(t)$.

Branch 1 is always unstable, so that for $\sigma_M > \Sigma > \sigma_m$ the system fluidity evolves either to 0 (again leading to creep, not to steady flow) if the initial value of a is smaller than $a_1(\Sigma)$, or toward $a_2(\Sigma)$ in the opposite case. Note that such a behavior is rather similar to the recently reported “viscosity bifurcation” [32]. This similarity remains if the constraint of homogeneity is lifted as will be discussed in Sec. IV. The stable branches 0 and 2 correspond, respectively, to stable nonflowing and flowing states of the system under Σ .

For larger stresses $\Sigma > \sigma_M$ branch 0 is unstable and the fluidity always evolves toward $a_2(\Sigma)$.

Eventually we note that for $\sigma_M > \Sigma > \sigma_m$ the addition of noise to the equation describing the evolution of a could lead the system to select either branch 0 or branch 2, depending on which one corresponds to the lowest value of V_Σ (the noise could allow the system to jump to the more favorable well, although possibly after very long times). Comparing these two values leads to the introduction of a value σ^* that will prove important in the following: for $\sigma_m < \Sigma < \sigma^*$, $0 = V_\Sigma(0) < V_\Sigma(a_2)$ so that branch 0 is the absolute minimum; for $\Sigma > \sigma^*$ branch 2 is the minimum. Formally, σ^* is given by $V_{\sigma^*}(a_2(\sigma^*)) = 0$ (see Fig. 5).

B. Imposed shear rate $\dot{\Gamma}$

Although the steady-state solutions are obviously the same as in the previous case, the dynamics is more complex when $\dot{\Gamma}$ is fixed, as it is governed by the coupled equations for the evolution in time of $\Sigma(t)$ and $a(t)$.

The stability of the steady-state solutions can, however, be examined by linearization around these solutions. The two stable branches 0 and 2 in Fig. 4 described in the case of an imposed stress remain stable. The stability of the decreasing branch 1 at fixed shear rate and with homogeneity imposed depends on the choice of the functions f and h in Eq. (6) (recall that as mentioned in Sec. II B we have formally suppressed the mechanical inertial mode of destabilization). For general f and h , one cannot preclude destabilization of the steady solution (1) to a limit cycle [33]. However, this is not the case with the expressions of Sec. II A $f(a)=ra^2+a^4$ and $h(a)=r'a+a^2$, for which the branch 1 is always stable (again when homogeneity is enforced).

IV. HETEROGENEOUS FLOW AT IMPOSED STRESS Σ

The situation at imposed fixed stress can be apprehended rather simply starting from the analysis of the homogeneous case mentioned above with its two stable branches 0 and 2. Heterogeneities are generated by the walls, which induce wall layers of different fluidities, with a major effect on the selection of the steady-state flow branch.

A. Imposed fluidity at the wall

We start by considering the case where the walls impose the local value of the fluidity $a|_{z=0,H}=a_w$. The evolution of the system is described by that of $a(z,t)$ from which the shear rate can easily be deduced, $\dot{\gamma}(z,t)=a(z,t)\Sigma$. Formally,

$$\frac{da}{dt} = - \frac{\delta F_\Sigma}{\delta a(z)} \tag{9}$$

which is a rather classical equation describing the local relaxation of a “free energy” $F_\Sigma(a(z))$. Here this functional is

$$F_\Sigma(a(z)) = \int_0^H \left[V_\Sigma(a) + \frac{1}{2} D(\partial_z a)^2 \right] dz, \tag{10}$$

where it is implicitly understood that a equals a_w on the boundaries.

The evolution can be understood as a minimization of F_Σ , as $d_t F_\Sigma = - \int_0^H dz (\partial_t a)^2 < 0$. Schematically, minima correspond to adopting throughout the sample a value of a minimizing V_Σ [i.e., 0 or $a_2(\Sigma)$], and then connecting at the boundaries to the imposed value a_w with a minimal penalty obtained as a compromise between the V_Σ term and the square gradient term (a more formal description of these steady-state solutions is given in the Appendix). This leads to steady-state branches in the $(\Sigma, \dot{\Gamma})$ plane that deviate from the branches 0 and 2 only by the contribution of these wall layers, which shifts the average shear rate by a small term proportional to ℓ/H , where $\ell \sim [Da_w/f(a_w)]^{1/2}$ is the thickness of these layers.

The stability of these branches is now limited by the fact that the walls at a_w can act as nucleating sites for the other phase. For example the “frozen” branch, where fluidity decreases from a_w on the wall to almost zero in the middle,

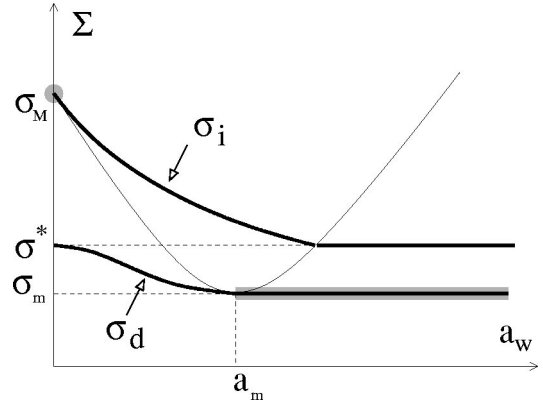


FIG. 6. Threshold values σ_i and σ_d of the stress as a function of the fluidity at the walls a_w . Above σ_i the frozen branch is unstable; below σ_d the fluidized branch is unstable. When the imposed macroscopic stress Σ is between σ_d and σ_i , both branches are stable. Which one is selected depends then on the initial conditions, i.e., on the system’s history. Areas in gray correspond to bulk destabilization (“spinodal”), whereas a simple thick line denotes destabilization from the wall (“heterogenous nucleation”).

ceases to be stable if Σ is increased so that it becomes interesting (in terms of minimizing F_Σ) to increase a beyond a_w at the expense of a section of the $a=0$ central part. The threshold roughly corresponds to $V_\Sigma(a_w) = V_\Sigma(0)$ which defines a maximal value of the stress $\sigma_i(a_w)$ for stability on the pasty branch. Beyond this value, the $a(z)$ solution “slips” into the potential well of branch 2. Similarly, the fluid branch ceases to be stable upon decrease of the stress Σ when the latter reaches the value $\sigma_d(a_w)$ defined by $V_{\sigma_d}(a_w) = V_{\sigma_d}(a_2(\sigma_d))$. It is easy to check that $\sigma_m \leq \sigma_d \leq \sigma^*$, whereas $\sigma^* \leq \sigma_i \leq \sigma_M$. Typical curves for $\sigma_i(a_w)$ and $\sigma_d(a_w)$ are plotted in Fig. 6.

A second process of destabilization exists. If the wall fluidity has extreme values (either low or high) walls may no longer be involved in the destabilization process, which is then “spinodal” (gray areas in Fig. 6).

The conclusion for the macroscopic steady-flow $\Sigma(\dot{\Gamma})$ diagram is thus simple. At fixed Σ there are two stable flow curves. For $\Sigma < \sigma_i(a_w)$ a branch exists close to the axis corresponding to a frozen bulk with two layers of finite fluidity close to the walls (as schematized, e.g., in Fig. 2). This branch is indistinguishable from the vertical axis for large values of the thickness H . For $\Sigma > \sigma_d(a_w)$, a fluidized branch exists very close to 2 (identical in the limit $H \rightarrow \infty$), with a flowing bulk, and slightly less fluid wall layers.

In the intermediate range $\sigma_d < \Sigma < \sigma_i$, both branches are stable. The branch actually selected depends on the system history and preparation (initial conditions). This is very compatible with recent observations of a “bifurcation” of the asymptotic viscosity at a given value of the applied stress for a given preparation [32].

If one starts with macroscopic bands of fluidized and frozen material, the fronts between these zones will move so that one typically ends on the fluid branch for $\Sigma > \sigma^*$ and on the frozen branch for $\Sigma < \sigma^*$.

If the stress Σ is varied slowly in a systematic way (i.e.,

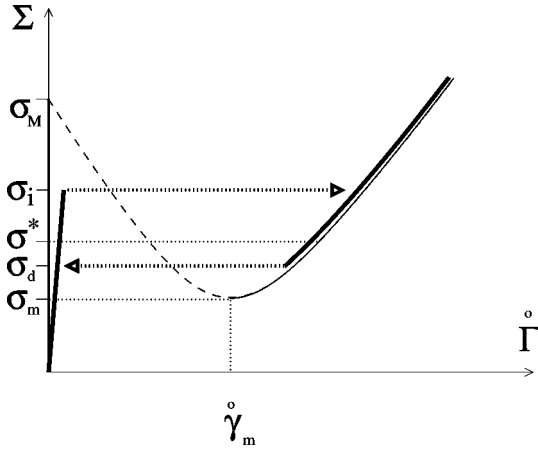


FIG. 7. Macroscopic flow curve at imposed stress Σ (thick lines). The thin lines (dashed and continuous) correspond to the local flow curve of Fig. 2. The value of the fluidity a_w at the walls fixes the location of the limits of stability σ_i and σ_d of the frozen and fluid branches (see Fig. 6). When the stress is varied monotonically, the shear rate suddenly jumps at these values (thick arrows).

increased or decreased), one has the simple hysteretic behavior described by the thick arrows in Fig. 7.

The departure from the homogeneous case described in the previous section is due to the walls, which introduce the parameters H and a_w . Although the former has a moderate role in shifting by a small amount the branches in the diagram (by a term proportional to ℓ/H), the latter controls the position of the instability thresholds, and thus the amplitude $\sigma_i - \sigma_d$ of the hysteresis loop observed macroscopically. (Actually, looking at the details, these threshold stresses depend very slightly on H but this effect is almost invisible numerically. See the Appendix).

The above picture (Fig. 7) is confirmed by numerical simulations by starting from various arbitrary initial conditions and also by submitting the system to ramps of increasing and decreasing stress. These simulations also allow one to follow the destabilization process. Starting from a frozen solution, the bulk is destabilized when $\Sigma = \sigma_i$. This destabilization process is initiated at the wall, where the fluidity is fixed and nonvanishing (acting therefore as a destabilizing nucleus): two fronts of large fluidity are first created at each wall, and then propagate in the material to merge eventually at the middle of the Couette cell to give the homogeneous $a_2(\Sigma)$ bulk solution (Fig. 8).

On the other hand, starting from the fluidized branch, when the stress is decreased this highly sheared solution is destabilized for $\Sigma = \sigma_d$. The destabilization process depends on a_w . If $a_w < a_m$, then $\sigma_d > \sigma_m$ and the destabilization occurs by fronts merging, as previously described, whereas in the reverse case $\sigma_d = \sigma_m$, and the bulk is destabilized as a whole, as a plateau decreasing in time toward zero.

Note that the problem is formally very similar to that of wetting transitions in thermodynamics: it reduces to the minimization of a free energy functional that is the sum of squared gradient term $(\partial_z a)^2$ and a potential with two wells $V_\sigma(a)$, with boundary conditions on the walls that can favor one or the other of the phases.

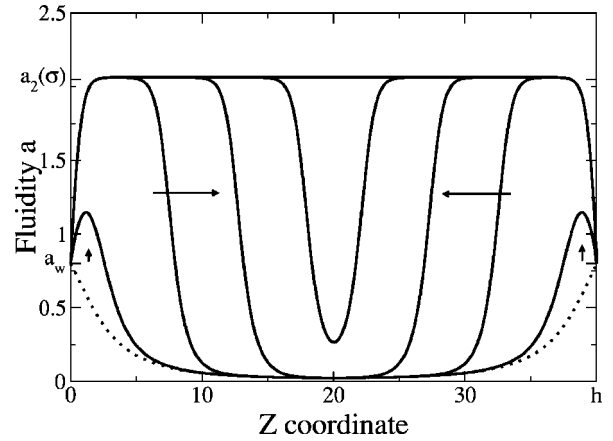


FIG. 8. Destabilization of the frozen bulk by heterogeneous nucleation. The initial state is plotted with dotted lines. As the stress is increased so that $\Sigma \geq \sigma_i$, two fronts come from the walls, as shown by the arrows, before they merge in the center. The steady state is the fluidized bulk. In this simulation $f(a) = a^2 + a^4$, $h(a) = 0.05a + a^2$, $a_w = 0.8$, and $\Sigma = 1.45$.

In this interpretation, the sections $\sigma^* \rightarrow \sigma_i$ on the pasty branch and $\sigma_d \rightarrow \sigma^*$ on the flowing one would be called metastable. The absence of noise in the equations used here makes them absolutely stable. Adding some noise in the bulk equation for a would reduce the metastable branch, bringing the system (possibly after prohibitively long waiting times) to jump from the pasty to the fluid branch at σ^* .

Note that it may be experimentally difficult to detect the hysteresis loop if its amplitude is small (either because $\sigma_i - \sigma_d$ is small or because of the presence of noise), which would make this macroscopic flow curve very similar to a textbook description of a fluid with a yield stress σ^* , with possibly a rather abrupt change of the steady-state shear rate at this value.

B. No flux at the wall: $\partial_z a|_{z=0,H} = 0$

If the boundary conditions are such that $\partial_z a = 0$ on the walls, then the behavior of the system is exactly that obtained in the analysis of the homogeneous model: the system tends to relax any inhomogeneity, and its stable steady-state solutions are those of the homogeneous model, a pasty branch 0 for $\Sigma < \sigma_M$ and a fluid branch 2 for $\Sigma > \sigma_m$. Both branches are stable solutions for $\sigma_m < \Sigma < \sigma_M$. It results in a hysteretic loop of amplitude larger than in the previous case.

So the picture is still quite similar to Fig. 7 above with the following differences: here $\sigma_i = \sigma_M$ and $\sigma_d = \sigma_m$, and the branches follow the local flow curve strictly, with no slight deviation due to wall layers.

Again we have checked the validity of this picture numerically.

V. HETEROGENEITIES AT IMPOSED SHEAR RATE $\dot{\Gamma}$

We now turn to the case where the global shear rate is controlled, i.e., the velocity V of the top wall is fixed, so that

the average shear rate $\dot{\Gamma}$ is imposed. The dynamics of the system is now more complex and governed by two coupled integro-differential equations, that can be obtained from Eq. (6):

$$\begin{aligned} \partial_t \Sigma &= -\langle a \rangle(t) \Sigma(t) + \dot{\Gamma}, \\ \partial_t a &= -f(a) + ah(a) \Sigma^2(t) + h(a) \Sigma \partial_t \Sigma + D \partial_{zz}^2 a, \end{aligned} \quad (11)$$

where $\langle a \rangle$ is the spatial average of $a(z, t)$,

$$\langle a \rangle(t) = \frac{1}{H} \int_0^H dz a(z, t), \quad (12)$$

and where the boundary conditions are either $a|_{z=0,H} = a_w$ or $\partial_z a|_{z=0,H} = 0$. The local shear rate is given by $\dot{\gamma}(z, t) = \dot{\Gamma} + [a(z, t) - \langle a \rangle(t)] \Sigma$.

This set of dynamic equations leads to a much richer set of situations, as the dynamics of a does not relax a free energy [formally, $\partial_t a = -\delta F_{\Sigma(t)} / \delta a(z) + \frac{1}{2} h(a) \partial_t \Sigma^2$]. As a result, for some values of $\dot{\Gamma}$, the system can have many steady states corresponding to different values of Σ , and for some others none [the system then tends to a limit cycle corresponding to a periodic solution for $a(z, t)$ and for $\Sigma(t)$ that yields a macroscopic stick-slip behavior].

To explore this ensemble of scenarios it is necessary to solve these equations numerically. Our numerical exploration leads to a complex picture. Starting with the case of a fixed fluidity at the walls, we first describe the main features observed, before pointing out more complex features, including the metastability of various patterns of shear bands and the occurrence of localized oscillations. At this stage we have no analytical understanding of some of these features, and of their dependence on the parameters. The behaviors reported here result from numerical simulations with f and h fixed to $f(a) = ra^2 + a^4$ and $h(a) = r'a + a^2$. At the end of this section we turn to the case of zero fluidity gradient at the walls to underline a few differences from the previous case.

A. Imposed fluidity at the wall

We start by analyzing the case where the fluidity at the walls is fixed to a value a_w . Depending on $\dot{\Gamma}$ and a_w different behaviors are observed. The main features are the following. First, the frozen $0 < \Sigma < \sigma_i$ and fluidized $\sigma_d < \Sigma$ branches found at fixed stress (Sec. IV) are also found to be stable at imposed $\dot{\Gamma}$. Second, between two values $\dot{\gamma}_i$ and $\dot{\gamma}_d$ defined in terms of the threshold stresses on these branches (see Fig. 9), the most frequent long time behaviors (which we take as the steady states) are solutions corresponding to the coexistence of “bands” of frozen ($a \approx 0$) and fluidized phases [$a \approx a_2(\sigma^*)$] coexisting at a stress $\Sigma \approx \sigma^*$. Finally, in a narrow vicinity of the transition from the quasihomogeneous branches to this situation of coexisting “shear bands” (i.e., $\dot{\Gamma}$ slightly larger than $\dot{\gamma}_i$ or slightly smaller than $\dot{\gamma}_d$), various phenomena can occur in the vicinity of the wall: nucleation of thin layers of fluidity different from the bulk, or of layers of periodically oscillating fluidity.

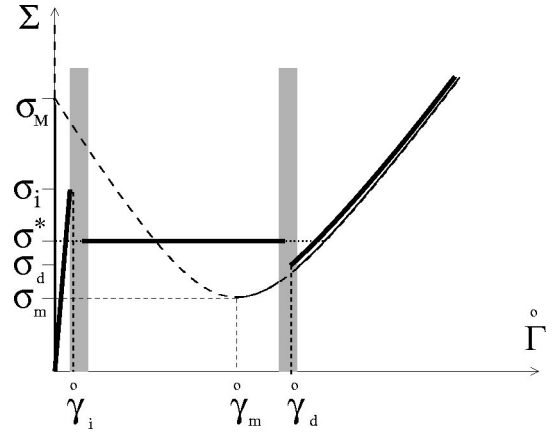


FIG. 9. Schematic macroscopic flow curve at imposed shear rate $\dot{\Gamma}$ (thick lines). Again the thin lines (continuous and dashed) denote the local flow curve. The value of the fluidity at the walls fixes the location of the limit shear rates $\dot{\gamma}_i$ and $\dot{\gamma}_d$ of the frozen and fluid homogeneous branches. Between these values the system tends to segregate into shear bands. At the transition between the two (gray areas), stable or oscillating thin layer structures are observed in the vicinity of the walls.

These behaviors have different signatures as shown on the macroscopic flow curve sketched in Fig. 9.

1. Frozen and fluidized regimes

First, for small and large imposed shear rate $\dot{\Gamma}$ one recovers the solutions obtained at imposed stress: except for small boundary effects, they correspond to the frozen branch 0, and to the fluidized branch 2 of the local flow curve.

Along the fluidized branch, the $\Sigma(\dot{\Gamma})$ relationship almost exactly follows the intrinsic flow curve obtained in the homogeneous case. The frozen branch actually displays an almost vertical section going to zero in the limit of vanishing shear rate $\dot{\Gamma} \rightarrow 0$ due to the presence of a small wall layer of finite fluidity imposed by the wall a_w and of thickness ℓ .

These domains are limited by the global stresses $\sigma_i(a_w)$ and $\sigma_d(a_w)$, as discussed in Sec. IV. The corresponding shear rates $\dot{\gamma}_i$ and $\dot{\gamma}_d$ can be calculated numerically with the method described in the Appendix.

2. Shear-banding regime

A shear-banding domain connects the two previous frozen and fluidized regions. It corresponds to a coexistence in the shear cell of the frozen and the fluidized states. Its signature on the macroscopic flow curve is a quasiplateau at a stress $\Sigma \sim \sigma^*$. All over the banding domain (for a given a_w), the stress is found to remain in the vicinity of the value σ^* defined in Sec. III by $V_{\sigma^*}(a_2(\sigma^*)) = V_{\sigma^*}(0)$. This approximately fixes the value of the fluidity in the fluidized region to $a^* = a_2(\sigma^*)$, with $a_2(\sigma)$ being the corresponding branch obtained in the homogeneous case (see Sec. III). The shear rate in the fluidized region is approximately given accordingly as $\dot{\gamma}^* = a^* \sigma^*$. The total width of the frozen and fluidized regions are determined by the global constraint on the

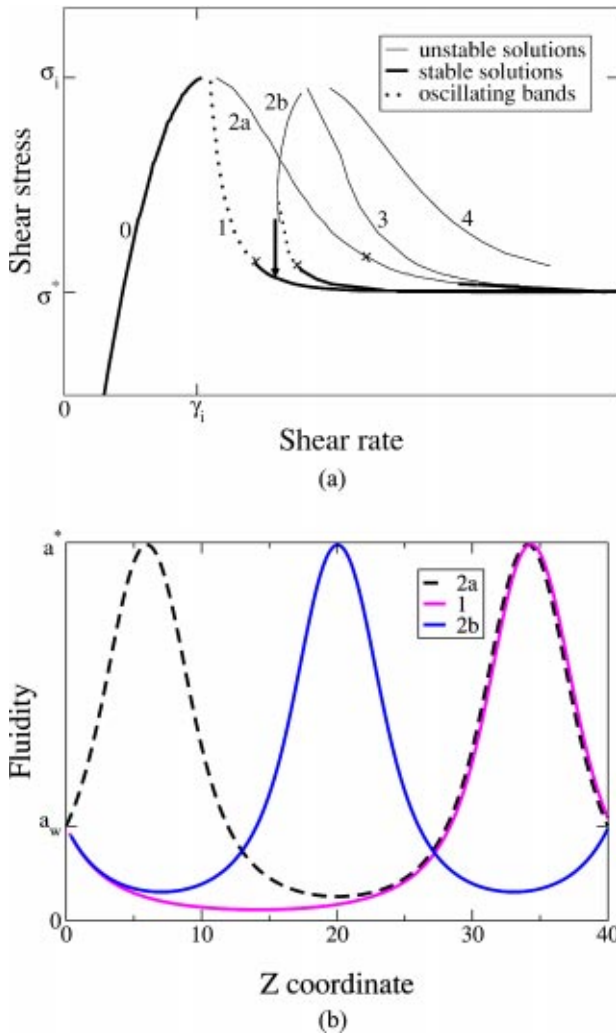


FIG. 10. (a) Calculated steady-state flow curves: the unstable stationary solutions are plotted with thin lines, the stable solutions with thick lines, and the oscillating solutions with dotted lines. The numbers on the branches represent the number of fronts between the fluidized and frozen bands. $r=1$, $r'=0.01$, $H=40$, $a_w=0.25$. (b) Fluidity profiles corresponding to the points marked with crosses on (a) for the branches 2a, 2b, and 1.

total shear rate. The width of the fluidized region h_f is typically given by $h_f \approx H\dot{\Gamma}/\dot{\gamma}^*$, with $\dot{\gamma}^*$ defined above (small boundary effects neglected).

An interesting question concerns the number of fluidized bands: how many fronts between a frozen and a fluidized band can be stabilized for given H , a_w , and $\dot{\Gamma}$? In order to answer this question, a zoom of the quasiplateau is plotted in Fig. 10(a) for given H and a_w . The stable quasiplateau actually consists of parts of the branches representing the steady-state solutions with several fronts (on the figure these stable parts of the branches are plotted with thick lines). The steady-state multifront branches were calculated numerically with the method detailed in the Appendix. The fluidity profiles corresponding to the branches with one and two fronts are represented in Fig. 10(b). Their stability was then examined with the numerical simulation described in Sec. II D.

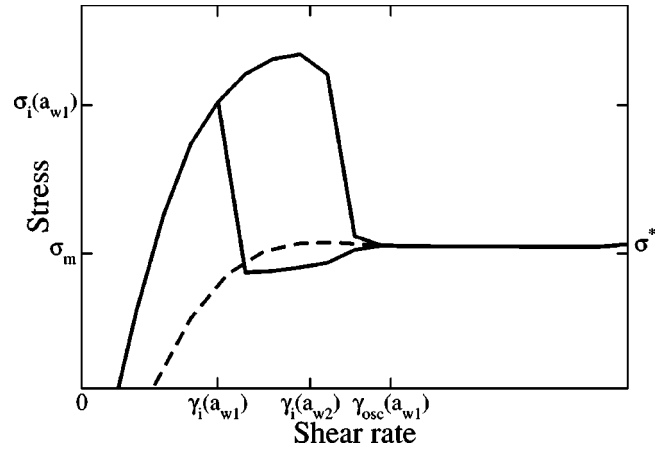


FIG. 11. Behavior at low shear rate for a fixed $H=100$, $r=1$, $r'=0.01$. The solid line corresponds to $a_{w1}=0.3$ and the dashed line to $a_{w2}=1$. In the case of a_{w1} , oscillations are observed, and the envelope of the oscillations is represented.

No analytical characterization was found to the limits of stability of the multifront branches. Beyond these limits, either oscillations are observed, or other stable branches are reached. Their complex dependence on a_w and Σ , is shown in Fig. 11. Note that, with the parameters taken to plot Fig. 10(a), for a small range of $\dot{\Gamma}$ [just left of the middle cross in Fig. 10(a)], two solutions are possible (depending on the history of the system): stable oscillations of a central fluidized layer (branch 2b), and a steady solution with a single fluid layer at the wall (branch 1). In the case of oscillations, when $\dot{\Gamma}$ is further decreased to the limit of stability of branch 2b, the system evolves toward the pattern of branch 1 as indicated by the arrow in Fig. 10(a).

3. Stick-slip behavior

When no stable branch is reached, a time dependent oscillating behavior is evidenced for stress and fluidity. As seen in Fig. 11, this occurs for small wall fluidity and imposed shear rate. This behavior is very reminiscent of stick-slip, a phenomenon commonly encountered in solid friction [33,34]. Here it originates in an oscillating behavior of the fluidity between a frozen state (stick phase) and a partially fluidized state (slip phase).

The fluidization however, occurs only within one layer, the rest of the system being frozen. This spatially localized oscillating behavior resembles a periodic fracture-healing process, as observed, e.g., by Pignon *et al.* [10]. The fluidized layer is localized either close to the wall, or in the middle of the shear cell, its fluidity oscillates between two extremal values, and its thickness is approximately constant. The time evolution of Σ and the maximum fluidity of the layer are plotted in Fig. 12, showing characteristic features of stick-slip behavior.

The system rapidly relaxes to the frozen state, i.e., a very small fluidity, while the stress increases until a limit where the fluidity abruptly increases, i.e., the fluid is suddenly sheared. This sudden increase is due to the penetration of the maximum fluidity in the basin of attraction of the fluidized

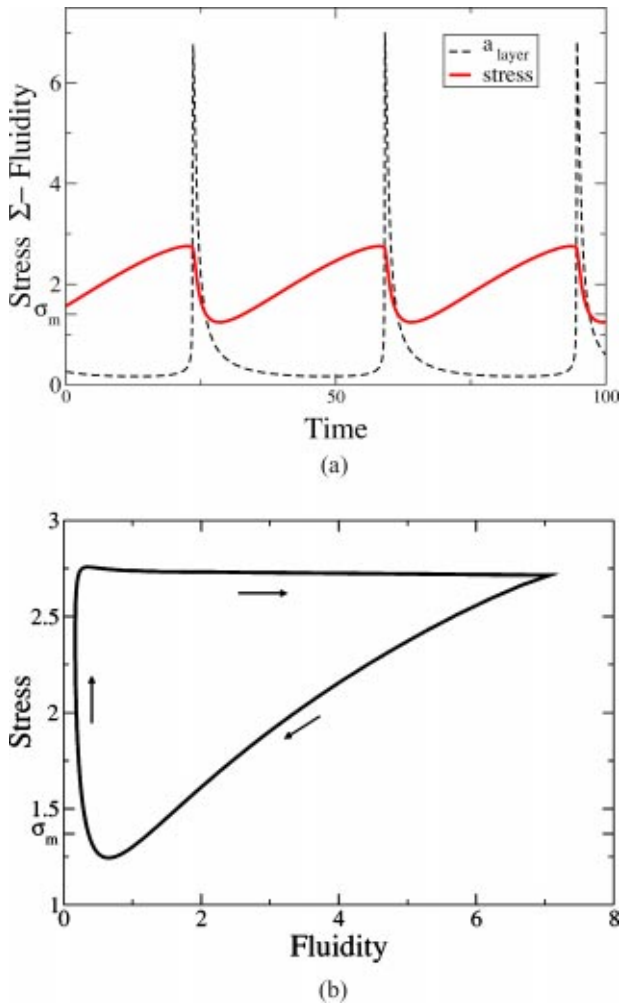


FIG. 12. The amplitudes of the oscillations of the global stress and of the maximum fluidity in the oscillating layer are represented as a function of time (a), and in the plane (a, Σ) (b), in the case $a_w=0.3$, $r=1$, $r'=0.01$, $\dot{\Gamma}=0.12$. Its width hardly varies.

solution $a_2(\sigma)$, which is enlarged as σ increases. To maintain a fixed global shear rate, σ relaxes quickly and the cycle starts again.

B. No flux at the wall: $\partial_z a|_{z=0, H} = 0$

In the case of a no flux boundary condition and for intermediate values of $\dot{\Gamma}$ ($\dot{\gamma}_i < \dot{\Gamma} < \dot{\gamma}_d$), two very different locally stable sets of solutions of Eqs. (11) and (12) are possible: one is very similar to the solutions obtained above for fixed fluidity at the walls and exhibits shear banding and stick-slip behavior; the other one is the homogeneous solution at fixed shear rate obtained in Sec. III. This peculiarity is associated with the specific form of the boundary condition, which is compatible with a homogeneous fluidity in the cell. Moreover, as discussed in Sec. III, the decreasing branch is linearly stable at fixed shear rate (remember that we have suppressed inertial terms), and no destabilizing mechanism is induced here by the boundaries (in contrast with the fixed wall fluidity case). Formally, the system is thus attracted either by the homogeneous solution or by the inhomogeneous

one, depending on initial conditions (an initial inhomogeneous state often leading to a banded inhomogeneous solution).

The macroscopic flow curve for Eqs. (11) and (12) with the present boundary conditions consists of the following:

(1) The two increasing branches of the local curve (the branches are parts of the local curve as the solutions are homogeneous). Those branches are also stable in the case of imposed stress.

(2) The decreasing branch of the local curve. This is of course an artifact due to our neglecting inertial terms, which suppresses the “mechanical instability” that always destabilizes this branch.

(3) The quasiplateau, with $\Sigma \sim \sigma^*$. As in the case of an imposed fluidity at the wall, it is constituted of parts of multifront branches, which become unstable at different values of the shear rate.

(4) An oscillating domain, for small shear rates, when the single front branch loses its stability.

Ruling out the unphysical decreasing branch, the picture is thus quite similar to Fig. 9 (without the effective wall slip in branch 1 due to the finite wall fluidity there).

C. Comment on the oscillations

Oscillating response under steady driving has recently been numerically observed in a model for shear-thickening materials [35], which in contrast to the present one described the homogeneous behavior of a system (no spatial heterogeneity in the formalism), and the oscillations were shear-rate oscillations at fixed stress. Formally there are some similarities as in both cases a continuous (and thus infinite) set of variables evolves through coupled differential equations with nonmonotonic functions involved, and driven by a global integral constraint. However, in contrast to the situation of [35] where all the variables were involved in the oscillation, here only a limited set of variables are (corresponding to a spatially localized oscillating layer).

In principle a finite number of variables is enough to get an oscillating rheological response (limit cycles) under steady driving [36], so it is no surprise that oscillations show up here given the complexity of the set of equations (11),(12) and the number of variables involved. One may even expect more complex dynamical behavior such as some form of chaotic response [36], but we found none within the set of parameters numerically explored. Clearly, a truly three-dimensional version of this model, with the corresponding nonlinear convective terms, should increase the likeliness of chaotic behavior (even in the absence of inertia [37]).

VI. DISCUSSION

In the present paper we used an extension of a model previously introduced to account for the rheology and aging in pasty systems, in which the steady-state local flow curve is nonmonotonic so that heterogeneous flows can be generated at steady state. The key ingredient of the model is a coupling between the mechanical variables, namely, shear stress or shear rate, and local relaxation within the fluid, characterized

by a fluidity. Although analytically very simple, the model yields a rather rich macroscopic phenomenology.

(1) Under controlled stress Σ , the steady-state behavior is schematized in Fig. 7. The fluid undergoes a hysteretic phenomenon if the stress is increased or decreased progressively. The effective yield stress is shown to depend on the fluid history and on the wall conditions. In addition, no banding is observed and there is a discontinuity in shear rate $\dot{\Gamma}$ which occurs at specific values of the stress.

In this case, we have shown that the dynamics reduces to the minimization of a free energy function. This is generalizable to any function f, g describing aging and fluidization, and to more complex diffusion terms $D(a)$. Note that the dynamics was not built as a free energy relaxation but naturally appears this way (see the related discussions in [13]). This gives some generality to the qualitative results, beyond the specific model studied here.

As no noise term was included, the equivalent of homogeneous nucleation in thermodynamics problem was suppressed and boundary conditions play a crucial role in destabilization processes. Hence, the values of the thresholds depend on the boundary conditions. However, the qualitative behavior (hysteretic loop) is rather insensitive to the specific type of boundary condition chosen.

(2) At fixed global shear rate $\dot{\Gamma}$, the macroscopic behavior is schematized in Fig. 9: banding solutions show up, separating a frozen region from a fluidized region. The shear rate within the fluidized band is hardly dependent on the imposed global shear rate, and fixed only by characteristics of the material. Within the banding domain, the thickness of the fluidized region increases (nearly) linearly with the global shear rate $\dot{\Gamma}$ to eventually fill the full shear cell.

At small (total) shear rate, an oscillating behavior of the stress Σ is observed, with features very reminiscent of a classical stick-slip behavior. The system is globally in a frozen state, and fluidizes periodically within a thin layer. Such a behavior compares well with the fracturing and healing process observed by Chen *et al.* [6] and Pignon *et al.* [10]. These localized oscillations are to be contrasted with homogeneous oscillations obtained in other models for different systems (e.g., [35]).

Our observations result from numerical simulations and the influence of the specificity of the modelization of the fluidization and aging remains to be understood. Again, the different thresholds depend on the boundary conditions, but the qualitative behaviors described are robust to changes in the types of boundary conditions. Extension of the present model to a fully three-dimensional description could, however, yield a more complex dynamical behavior.

In conclusion, we suggest that analyzing yield stress fluids close to the yield stress at both constant stress and constant shear rate could provide interesting information. It could also be informative to check the sensitivity of the results to the nature of the surfaces bounding the fluid.

APPENDIX: STATIONARY SOLUTIONS OF EQ. (6)

In this appendix, we detail the steady-state solutions of Eq. (6) recalled here:

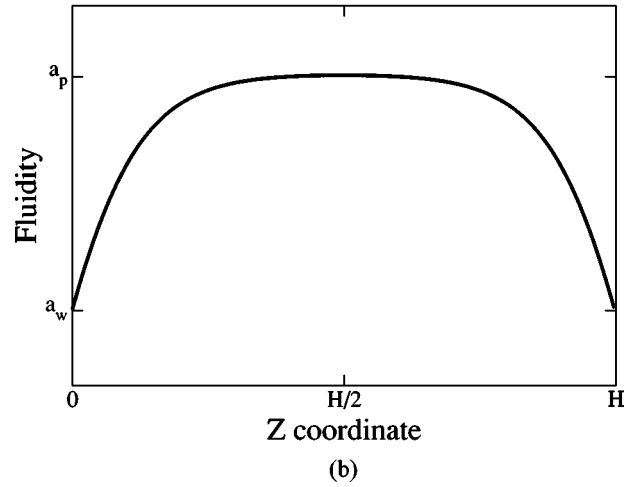
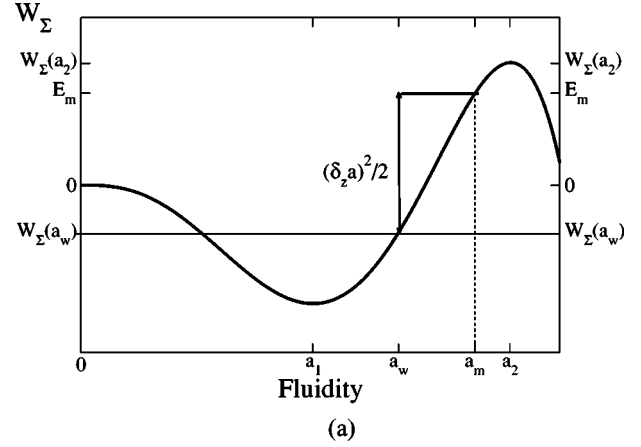


FIG. 13. (a) Potential W_Σ . $\Sigma = 1.44$, $r = 1$, $r' = 0.01$. (b) Fluidity profile for a fluidized bulk. $a_w = 1$, $H = 15$.

$$a(z)\Sigma = \dot{\gamma}(z),$$

$$-f(a(z)) + a(z)h(a(z))\Sigma^2 + D\partial_{zz}^2 a(z) = 0,$$

$$a|_{z=0,H} = a_w \quad \text{or} \quad \partial_z a|_{z=0,H} = 0. \quad (\text{A1})$$

For clarity, the potential $W_\Sigma(a)$ is introduced as $W_\Sigma(a) = -\int_0^a da' [f(a') - a' h(a') \Sigma^2]$. Note that $W_\Sigma = -V_\Sigma$ as defined in Eq. (8). Hence for a given Σ we look for a solution $a(z)$ such that

$$-\partial_a W_\Sigma(a) = D\partial_{zz}^2 a(z),$$

$$a|_{z=0,H} = a_w \quad \text{or} \quad \partial_z a|_{z=0,H} = 0. \quad (\text{A2})$$

The local shear rate is then immediately deduced: $\dot{\gamma}(z) = a(z)\Sigma$.

Equation (A2) can be interpreted as the classical equation of motion of a particle of mass D and position a in the potential W_Σ where z plays the role of time. The energy $E_m = \frac{1}{2}(\partial_z a)^2 + W_\Sigma(a)$ is conserved during the motion.

With this interpretation, the boundary conditions impose initial and final positions (a_w imposed at the walls) or velocities ($\partial_z a = 0$ imposed at the walls).

We choose to detail here the case of an imposed a_w at the wall, and the stress Σ is chosen $\sigma_i > \Sigma > \sigma_d$ (see Sec. IV).

The potential W_Σ is represented in Fig. 13. The extreme values of the mechanical energy E_m are $W_\Sigma(a_w)$ and $W_\Sigma(a_2)$. From the analysis of these solutions, it is possible to progress further in answering a few questions.

(1) *What is the fluidity profile on the frozen and fluidized branches of Figs. 7 and 9?* For a given thickness H , E_m is set so that $a|_{z=0,H} = a_w$ with $\partial_z a|_{z=0} > 0$. With the mechanical analogy, this amounts to fixing the mechanical energy or initial velocity for the particle to leave position a_w , reach a maximum a_m with $\partial_z a|_{a_m} = 0$, and go back to its initial position within a time H .

The fluidity profile is represented in Fig. 13. Note that $E_m = W_\Sigma(a_2)$ corresponds to a fluidized bulk, with an infinite thickness $H \sim \infty$.

With $\partial_z a|_{z=0} > 0$, a profile with a bulk of fluidity higher than a_w is described.

Symmetrically, a profile on the frozen branch, that is, with a bulk fluidity smaller than a_w is described by fixing $\partial_z a|_{z=0} < 0$, and following the same procedure.

(2) *What is the limit of existence for the fluidized bulk solution σ_i ?* $\sigma_i(H, a_w)$ was defined in Sec. IV as the stress beyond which a profile with a frozen bulk can not be observed.

For $H \sim \infty$, $\sigma_i(\infty, a_w)$ is defined by $W_{\sigma_i}(a_w) = 0$. With the mechanical analogy, the mechanical energy E_m is set to 0, that is, the particle leaves its position a_w with a velocity $\partial_z a|_{z=0} \sim 0$, and spends an infinite time at the position $a_m = 0$.

For $\sigma > \sigma_i$, $W_\sigma(a_w) > 0$, and for $a < a_w$, $W_\sigma(a) < W_\sigma(a_w)$. With the mechanical analogy, the particle cannot leave the position a_w with a negative velocity and come back to it after a time H . There is no solution with a frozen bulk.

For a finite H , a frozen bulk requires $E_m \leq 0$; therefore $\sigma_i(H, a_w)$ is slightly smaller than $\sigma_i(\infty, a_w)$, by an amount that scales as H^{-3} .

The situation is symmetric for the definition of $\sigma_d(H, a_w)$, which is found to be slightly larger than $\sigma_d(\infty, a_w)$.

(3) *How can one calculate the fluidity profile for a solution with several bands?* The mechanical energy E_m is now decreased from $\min[W_\Sigma(0), W_\Sigma(a_2)]$ to $W_\Sigma(a_w)$ to find banded stationary solutions: a frozen bulk solution with thickness h_1 and, a fluidized bulk solution with thickness h_2 (both with the same energy E_m) such that $h_1 + h_2 = H$ form together a single interface solution. The same process is derived to find multibanded solutions. Solutions of Fig. 10 were calculated numerically with this method.

-
- [1] M. M. Britton and P. T. Callaghan, *J. Rheol.* **41**, 1365 (1997).
 [2] L. Ramos, F. Molino, and G. Porte, *Langmuir* **16**, 5846 (2000).
 [3] J. F. Berret, G. Porte, and J. P. Decruppe, *Phys. Rev. E* **55**, 1668 (1997).
 [4] O. Diat, D. Roux, and F. Nallet, *Phys. Rev. E* **51**, 3296 (1995).
 [5] G. Debrégeas, H. Tabuteau, and J.-M. di Meglio, *Phys. Rev. Lett.* **87**, 178305 (2001).
 [6] L. B. Chen, B. J. Ackerson, and C. F. Zukoski, *J. Rheol.* **38**, 193 (1994).
 [7] J. S. Raynaud, P. Moucheront, J. C. Baudez, F. Bertrand, J. P. Guilbaud, and P. Coussot (unpublished); P. Coussot, J. S. Raynaud, F. Bertrand, P. Moucheront, J. P. Guilbaud, H. T. Huynh, S. Jarny, and D. Lesueur, *Phys. Rev. Lett.* **88**, 218301 (2002).
 [8] P. Sollich, F. Lequeux, P. Hébraud, and M. E. Cates, *Phys. Rev. Lett.* **78**, 2020 (1997); P. Sollich, *Phys. Rev. E* **58**, 738 (1998).
 [9] M. Cloitre, R. Borrega, and L. Leibler, *Phys. Rev. Lett.* **85**, 4819 (2000); C. Derec, A. Ajdari, G. Ducouret, and F. Lequeux, *C.R. Acad. Sci., Ser. IV Phys. Astrophys.* **1**, 1115 (2000).
 [10] F. Pignon, A. Magnin, and J. M. Piau, *J. Rheol.* **40**, 573 (1996).
 [11] C. Barentin and B. Pouligny (unpublished).
 [12] J. K. G. Dhont, *Phys. Rev. E* **60**, 4534 (1999).
 [13] S. Butler and P. Harrowel, *Nature (London)* **415**, 1008 (2002).
 [14] P. D. Olmsted and C. Y. Lu, *Faraday Discuss.* **112**, 183 (1999).
 [15] P. D. Olmsted, *Europhys. Lett.* **48**, 339 (1999).
 [16] P. D. Olmsted and C. Y. D. Lu, *Phys. Rev. E* **60**, 4397 (1999).
 [17] O. Radulescu, P. D. Olmsted, and C. Y. Lu, *Rheol. Acta* **38**, 606 (1999).
 [18] J. L. Goveas and P. D. Olmsted, *Eur. Phys. J. E* **6**, 79 (2001).
 [19] P. Nozieres and D. Quemada, *Europhys. Lett.* **2**, 129 (1996).
 [20] G. Porte, J. F. Berret, and J. Harden, *J. Phys. II* **7**, 459 (1997).
 [21] C. Y. Lu, P. D. Olmsted, and R. C. Ball, *Phys. Rev. Lett.* **84**, 642 (2000), and references therein.
 [22] J. R. Pearson, *J. Rheol.* **38**, 309 (1994).
 [23] C. Derec, A. Ajdari, and F. Lequeux, *Eur. Phys. J. E* **4**, 355 (2001).
 [24] C. Derec, Ph.D. thesis, Université Paris VII, 2001.
 [25] J. Kurchan, e-print cond-mat/9812347.
 [26] D. Bonn, S. Tanase, B. Abou, H. Tanaka, and J. Meunier, *Phys. Rev. Lett.* **89**, 015701 (2002).
 [27] V. Schmitt, C. M. Marques, and F. Lequeux, *Phys. Rev. E* **52**, 4009 (1995).
 [28] L. Bocquet, W. Losert, D. Schalk, T. C. Lubensky, and J. P. Gollub, *Phys. Rev. E* **65**, 011307 (2002).
 [29] L. Bocquet and J.-L. Barrat, *Phys. Rev. E* **49**, 3079 (1994).
 [30] P. Scheidler, W. Kob, and K. Binder, e-print cond-mat/024164.
 [31] W. H. Press, B. P. Flannery, S. A. Teukolsky, and W. T. Vetterling, *Numerical Recipes in Fortran 90: The Art of Parallel Scientific Computing* (Cambridge University Press, Cambridge, England, 1988).
 [32] P. Coussot, Q. D. Nguyen, H. T. Huynh, and Daniel Bonn, *Phys. Rev. Lett.* **88**, 175501 (2002).
 [33] I. S. Aranson, L. S. Tsimring, and V. M. Vinokur, *Phys. Rev. B* **65**, 125402 (2002).
 [34] T. Baumberger, C. Caroli, and O. Ronsin, *Phys. Rev. Lett.* **88**, 075509 (2002).
 [35] D. A. Head, A. Ajdari, and M. E. Cates, *Europhys. Lett.* **57**, 120 (2002).
 [36] M. E. Cates, D. A. Head, and A. Ajdari, *Phys. Rev. E* **66**, 025202(R) (2002).
 [37] A. Groisman and V. Steinberg, *Europhys. Lett.* **43**, 165 (1998).